Squeeze Film Effects in MEMS Devices

Rudra Pratap, Suhas Mohite AND Ashok Kumar Pandey

Abstract | Squeeze film effects naturally occur in dynamic MEMS structures because most of these structures employ parallel plates or beams that trap a very thin film of air or some other gas between the structure and the fixed substrate. An accurate estimate of the effect of squeeze film is important for predicting the dynamic performance of such devices. In design, availability of very good models for squeeze film effects is indispensable. In this paper, we discuss the development of squeeze film flow modelling, tracking its routes to the air damped vibrating system studies in the early twentieth century. We try to capture the early developments in gas lubrication theory and then discuss the current developments motivated by the complexities in squeeze film flow analysis brought out by the geometries and flow conditions prevalent in dynamic MEMS devices.

CranesSci MEMS Lab, Department of Mechanical Engineering, Indian Institute of Science, Bangalore 560012, Karnataka, India
pratap@mecheng.iisc.ernet.in
mohitess@mecheng.iisc.ernet.in
ashok@mecheng.iisc.ernet.in

Keywords: MEMS, Squeeze-film damping, Reynolds equation, Rarefaction effect, Compressibility effect, Inertial effect, Perforations

Quality factor, Q: is 2π times the ratio of the total energy supplied divided by the energy lost in a single cycle. It is a measure of sharpness of the resonance peak.

1. Introduction

1.1. *Dynamic MEMS devices*

Ever since the realization of a silicon micro resonator[1], the number of dynamic MEMS structures and their applications have been steadily growing. The impetus for this growth is provided by the technological advances in microfabrication that enable us to make very fine suspended mechanical structures with varied topologies for realizing various kinds of in-plane, out-of-plane, and torsional oscillations. Typically, such structures have fairly high resonant frequencies, ranging from a few kHz to tens of MHz. Such high frequency devices, coupled with the ease of low-voltage electrostatic actuation and capacitive or piezoelectric sensing, find applications in inertial sensing, acoustic transduction, optical signal manipulation, and RF (radio frequency) components. Some important milestones in these application areas are the development of the Analog Devices integrated polysilicon ADXL accelerometers[2], flexural polysilicon micro gyroscopes[3], the 300-kHz micromechanical filters[4], MEMS torsional mirrors[5,6], Texas Instruments Digital Light Processing Chip (DLP)[7], AKU2000 MEMS microphone[8], ultrasonic motors[9], etc. All these devices employ one or the other type of vibrating micromechanical structures.

The most significant characteristic of a vibrating system is perhaps its resonant frequency response. A special measure that captures the most prominent feature of this response is called the *quality factor*, generally referred to as the *Q factor* of a device. The Q factor measures the sharpness of the resonant peak — a higher value indicating a sharper peak. It turns out that the Q factor is directly related to the overall damping present in the system. Thus, manipulation of the Q factor essentially involves manipulation of damping in the structure. There are several applications, especially in RF MEMS, where a very high Q factor is desired. MEMS technology has made it possible to build mechanical resonators with very high Q factors, so much so that they can replace some electronic components in RF applications on this singular merit. It has been shown that the quality factor of a polysilicon resonator can be as high as 10^6 if it is operated in vacuum[10]. However, not all devices can be vacuum packed. For example, acoustic transducers must work in a fluid medium. For other devices also, if the vacuum can be avoided without degrading the performance, it may be more cost effective to have the device operate in air

Figure 1: SEM pictures of various dynamic MEMS devices.

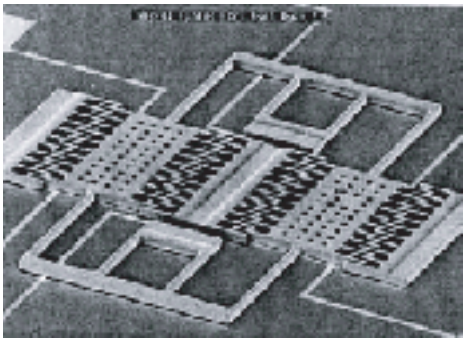

Tuning fork gyroscope: (Draper lab. www.draper.com/publications/draper25);

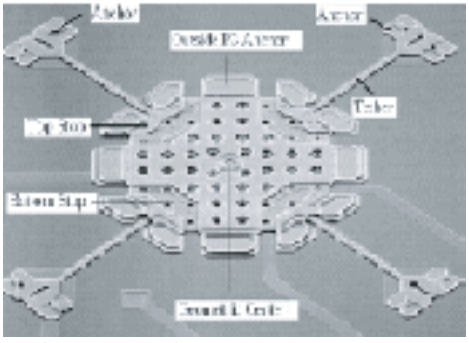

z axis MEMS accelerometer: (MOTOROLA MMA 1220D);

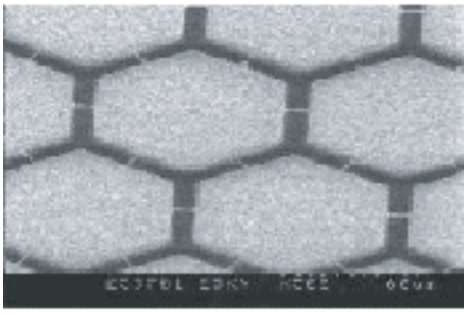

Capacitive ultrasonic transducer array, cMUT: (X. Jin et al., JMEMS 7(3) 1998);

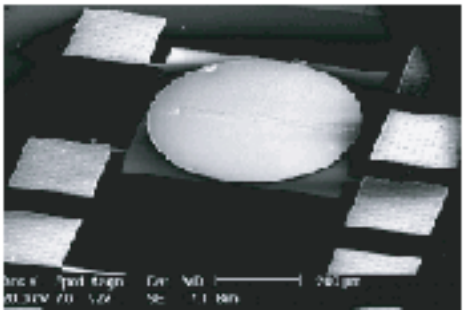

Micromirror,: (Bin Mi et al., JMEMS 14 (1) 2005);

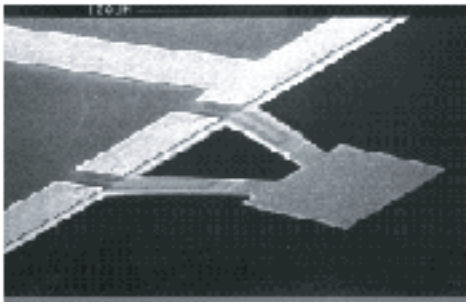

Micro resonator for detecting mass of biomolwcules: (N. Elejalde et al., MME 1999);

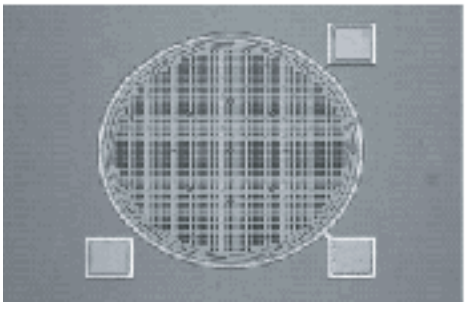

MEMS Microphone: (J. W. Weigold et al., Analog Devices Inc.2006);

or some inert gas filled packaging. However, the surrounding air or gas has significant effect on the dynamics of the device. What is special about this fluid interaction in MEMS devices is that the fluid is usually trapped under or around the vibrating micromechanical structures in extremely narrow gaps that necessitate the consideration of the fluid as a thin film, that is dynamically 'squeezed' by the vibrating structure. The complex interaction results in both damping and stiffening of the structure due to the fluid film. Modelling of this interaction and computation of the squeeze film effects under various conditions are the main topics of discussion in this paper.

Figure 1 shows pictures of some dynamic MEMS devices employing the principle of electrostatic sensing/actuation using the out-of-plane motion of a planar MEMS structure. Most of these devices have a thin film of air or some inert gas between the vibrating structure and the substrate. As the structure vibrates, it pushes and pulls the fluid film creating complex pressure patterns that depend on the geometry of the structure, the boundary conditions, perforations in the structure, frequency of oscillations, and thickness of the fluid film. As we show later, a reasonably accurate determination of the fluid pressure is key to computing squeeze film damping and stiffness. Although, there are

Figure 2: Schematic of a flexible structure under squeeze film damping.

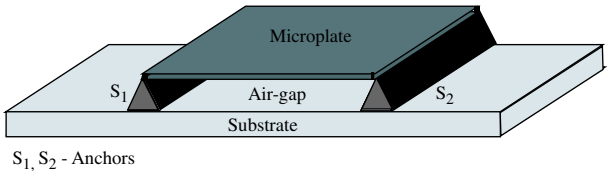

other damping mechanisms such as support loss, thermoelastic damping, etc., the squeeze film dominates when it is present, often by one or two orders of magnitude over the other damping mechanisms. Before we get into the modelling of squeeze film damping, we briefly review the relevant basic concepts of dynamic response and damping.

1.2. *Dynamic characterization*

As shown in Fig. 1, most dynamic MEMS devices employ microfabricated beam and plate structures. The squeeze film analysis in these structures is generally performed using the 2D isothermal compressible Reynolds equation coupled with equations governing the plate deflection[11,12]. Let us consider a microplate (Fig. 2) subjected to a time varying pressure $P_e(t)$ causing transverse motion of the plate. A squeeze film pressure $P_{sq}(x,y,t)$ develops underneath the plate due to its transverse motion pushing and pulling on the fluid film. Assuming small displacements and strains, we obtain the following equation governing the transverse motion of the plate

Damping factor, ζ: is the ratio of damping coefficient of a system to its critical damping coefficient.

$$\rho h_p \frac{\partial^2 w}{\partial t^2} + D\nabla^4 w - T\nabla^2 w = P_e(t) + P_{sq} \quad (1)$$

Figure 3: Computation of Q-factor from the frequency response curve of a resonator.

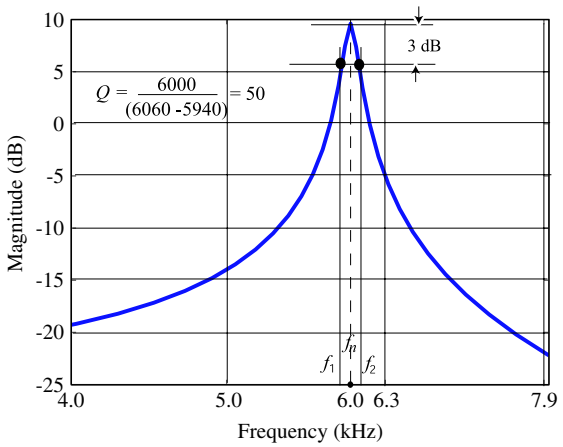

where $w(x,y,t)$ is the transverse deflection of a point (x,y) on the plate at time t, ρ is the plate material density, $D = \frac{Eh_p^3}{12(1-\nu^2)}$ is the plate flexural rigidity, h_p is the plate thickness, E is the Young's modulus, ν is the Poisson's ratio and T is the axial force per unit length. The pressure distribution $P_{sq}(x,y,t)$ in the squeeze film is governed by the Reynolds equation. The pressure boundary conditions for the air-gap in Fig. 2 are zero flux at the clamped edges of the plate and ambient pressure at the open edges. Thus, this analysis involves a coupled solution of equation (1) and the Reynolds equation (discussed later). Many MEMS structures, however, are generally assumed to be rigid, simplifying the coupled structural-fluid field problem to a single degree of freedom spring-mass-damper problem. This assumption also decouples the Reynolds equation, which leads to analytical solutions when linearized for small-amplitude oscillations. To characterize the performance of dynamic MEMS devices, an equivalent spring-mass-damper system under harmonic excitation is considered. The equation of motion is governed by

$$m\frac{d^2w}{dt^2} + c\frac{dw}{dt} + kw = F(t) \quad (2)$$

where, $k = k_s + k_a$ is the total stiffness—that of the structure and the *air spring*—and $c = c_s + c_a$ is the damping due to intrinsic losses in the structure and the viscous losses in the squeeze film. The structural spring constant, k_s, and damping constant, c_s, depend on the material and geometry and are, therefore, constant for a given system. In contrast, the air spring constant, k_a, and the damping constant, c_a, due to the fluid flow depend on the geometry, oscillation frequency and many factors which we discuss later.

If m is the equivalent mass (for a single degree of freedom model) of the oscillating structure and ω_n is its fundamental natural frequency, then the damping factor ζ is given by

$$\zeta = \frac{c}{c_c} = \frac{c}{2m\omega_n} \quad (3)$$

Equivalently, the quality factor Q is 2π times the ratio of the total energy supplied (E_{input}) divided by the energy lost (ΔE_{lost}) in a single cycle and is given by[13]

$$Q = 2\pi\frac{E_{input}}{\Delta E_{lost}} = \frac{m\omega_n}{c} \simeq \frac{1}{2\zeta}. \quad (4)$$

To calculate the quality factor directly from experimental results, we apply the half-width method (3 dB under the peak amplitude)[14]. The

Figure 4: A schematic diagram of squeeze film flow (A) downward normal motion; (B) upward normal motion.[20]

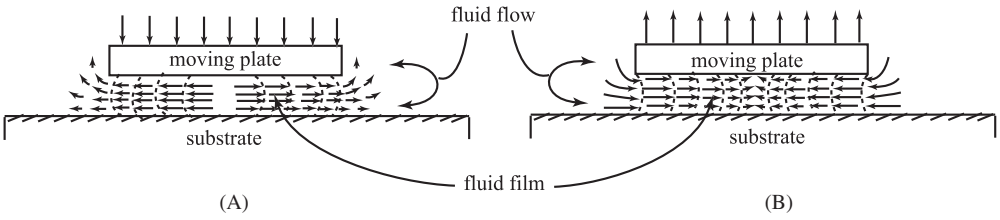

expression for the experimentally measured quality factor, Q_{exp}, is given by

$$Q_{\text{exp}} \approx \frac{1}{2\xi} = \frac{f_n}{f_2 - f_1} \tag{5}$$

where f_1 and f_2 are frequencies at which the amplitude of the displacement is equal to $1/\sqrt{2}$ times the maximum amplitude (equivalently, 3dB down), and f_n is the natural frequency in Hz. Figure 3 shows a typical frequency response curve of a resonator and the computation of its Q-factor.

1.3. *Dissipation mechanisms*

Different damping mechanisms are present in MEMS devices such as thermoelastic damping[15], support losses[16], and losses due to air flow[10,17]. The relative dominance of different damping mechanisms depends on the operating conditions and dimensions of the MEMS structures. To capture the cumulative effect of all type of loss mechanisms, the net quality factor Q_{net} is given by[18]

$$\frac{1}{Q_{\max}} \leq \frac{1}{Q_{\text{net}}} = \frac{1}{Q_{\text{ted}}} + \frac{1}{Q_{\text{support}}} + \frac{1}{Q_{\text{visc}}} + \ldots \leq \frac{1}{Q_{\min}}. \tag{6}$$

For most dynamic MEMS structures operating at ambient conditions, squeeze film damping is the most dominant damping mechanism[10,17–19]. This damping, however, can vary widely depending on the fluid pressure in the gap or the cavity. At very low pressures other damping mechanisms can become more dominant. Based on such considerations, Newell[19] has divided the pressure range into three main regions: the intrinsic, the molecular, and the viscous region. In the intrinsic region the ambient pressure is very low, so that the air damping is neglected compared to the intrinsic damping. In this region, damping is largely dependent on the surface to volume ratio, the surface quality and the material. In the molecular regime, damping is caused by independent collisions of non-interacting molecules. In this case, there is little interaction between the molecules. In viscous region, the pressure is high such that the air molecules also interact among themselves causing viscous effect.

Since the performance of any dynamic device is limited by the dominant damping mechanism in the system, we now discuss the theory of squeeze film damping, which is the dominant damping mechanism in most dynamic MEMS devices not operating in vacuum.

2. Squeeze film damping mechanism

When a planar structure oscillates normal to the substrate, the air-film between the structure and the substrate is squeezed causing a lateral fluid motion in the gap. Therefore, there is a change in pressure in the gap due to the viscous flow of air as shown in Fig. 4. The forces due to the built-up pressure are always against the movement of the structure. The work done in the viscous flow of air is transformed into heat. Thus, the air-film acts as a damper and the phenomenon is called squeeze film damping[21].

The squeeze film damping is basically prevalent in systems in which the air-gap (cavity) thickness is sufficiently small compared to the lateral dimensions of the structure. For smaller air-gap thickness, damping is higher while for larger gap it is negligible (viscous drag due to air flow on the surface becomes dominant for larger gaps). For a given value of air gap thickness, there are various factors that affect squeeze-damping, for example, the operating frequency of oscillations, surrounding pressure, boundary conditions, etc[22,20].

2.1. *Squeeze film damping in lubrication theory*

A large part of squeeze film flow analysis comes from the literature on lubrication theory. Researchers in this field were interested in understanding the mechanics of very thin fluid films between rotating or squeezing shafts and journal as well as thrust bearings. This problem was intensively investigated in sixties. While load bearing capacity of these

Figure 5: Frequency response curves obtained by analytical (—-) and FEM simulations (marked) for a 2D squeeze film damper of 80×80 μm square plate separated by a 5μm air-gap (h_a); the response curves without inertial effects are also shown (– · –) T. Veijola.[50]

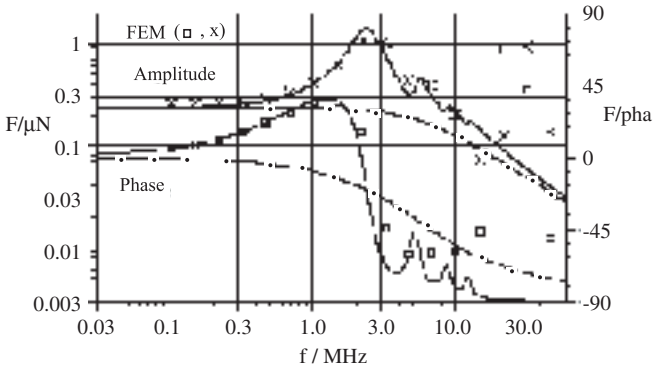

films under dynamic conditions was of central interest in these studies, the analysis naturally led to damping calculations and the effect on the dynamic response of the systems under investigation. Good mathematical models were developed for determining the squeeze film damping by many researchers[23–27]. The following two decades saw very little work or interest in this problem. However, the arrival of dynamic MEMS devices in the late eighties rekindled the interest in this subject. MEMS devices presented a new application with some new twists and turns in the problem. Naturally, there has been a lot of work in this area ever since. Although the central interest in the new studies is on damping characteristics of the squeeze film flow because of its direct bearing on the Q factor of a MEMS device, the dynamic spring characteristics of the film occupy center stage when the frequency of oscillation becomes considerably high. Several mathematical models exist today for the computation of both damping and spring effects of the film for various geometric and flow conditions. The applicability and validity of these different models are under continuous investigation because of continuous changes in device geometries and differences in experimentally observed results and predictions of theoretical models. The governing fluid flow equation used in most of these studies are either the linearized Reynolds equation in continuum region[26,27] or the modified Reynolds equation considering *slip flow* using Burgdorfer model[28].

Knudsen number, Kn: is the ratio of mean free path λ of gas molecules to the characteristic flow length. It is a measure of gas rarefaction.

One of the most significant effects present in squeeze film flow in MEMS structures is that of rarefaction. This effect arises because of the extremely small gaps in which the air or gas is forced to flow. Knudsen number, Kn, defined as the ratio of the mean free path of the gas molecules to the characteristic flow length, provides a very good measure of rarefaction. A very small value of Kn ($\ll 1$) usually results from large flow lengths and hence a situation where no molecular attention is required; continuum flow theory does very well. On the other hand, a large value of Kn (> 1) necessitates the consideration of molecular motion and attention on molecular interactions. In such rarefied flows, the classical assumption of zero relative velocity between the fluid molecules and the structural walls breaks down and consideration of slip flow at the wall becomes necessary. Slip flow conditions, however, are not unique to MEMS devices. These conditions were also observed and analysed by the researchers interested in gas lubrication theory.

Burgdorfer[28], who first introduced the concept of kinetic theory of gases to the field of gas-film lubrication, proposed a slip flow boundary condition at the walls by expanding the velocity near the wall in Taylor series. He retained the zeroth and first order terms to be used in the existing Reynolds equation for very small values of Knudsen number, Kn $\ll 1$. Hisa and Domoto[29] proposed a higher order approximation for Knudsen numbers larger than the range of Burgdorfer's equation by considering both the first and second order slip velocities together. Mitsuya[30] proposed a fractional (one and a half) order slip flow model. These models are based on the assumption of low Knudsen number, i.e., Kn $\ll 1$. Therefore, there was a need for a more general model to cover a wide range of Knudsen number that could account for ultra thin gaps. Gans[31], was the first to modify the existing Reynolds equation by describing the flows (i.e., Poiseuille flow, Couette flow, etc.) in terms of the linearized Boltzmann equation. To establish the validity of Gans's approximation for arbitrary Knudsen number, Fukui and Kaneko[32], analyzed it numerically and examined the lubrication characteristics. They found that Burgdorfer's modification overestimated the load carrying capacity with the first order velocity slip boundary condition in the Reynolds equation, and that underestimated it with one-and-a-half and second-order velocity slip boundary condition. After validating the Gans's approximation, Fukui and Kaneko[33] proposed the use of a Poiseuille flow rate database that they created by numerical calculation based on the linearized Boltzmann equation. They used the database effectively to reduce enormous calculations required to solve Boltzmann equation with the same accuracy ($\pm 1\%$) for a very small range of Knudsen number.

Another complication that arises because of the ultra thin fluid films is the effect of surface roughness

Figure 6: Variation of non-dimensional damping force (f_d/ϵ) and spring force (f_s/ϵ) with squeeze number σ; the point of intersection of the two curves (i.e., f_d=f_s) corresponds to the cut-off squeeze number (σ_c).

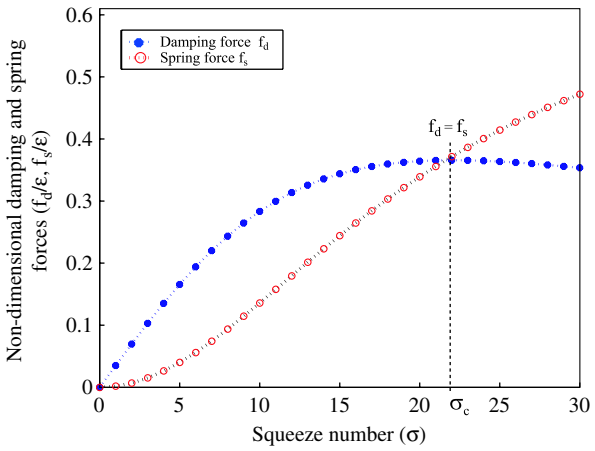

on the flow characteristics. To model this effect, Patir and Cheng[34], derived the average Reynolds equation by averaging the flow. The average flow rate is expressed as the rate of flow passing through averaged spacing, multiplied by an appropriate flow factor. The flow factor adjusts the Reynolds equation to give the correct average pressure and flow condition. These flow factors are obtained by numerical calculations using a small control area with a given surface roughness. The average flow model can be easily applied to distributed roughness problems. Elrod[35] tried to generalize the flow factors analytically. Tripp[36] outlined the mathematical method using perturbation approach with Greens function technique. Tonder[37] has shown analytically that the flow factors found to express roughness effects for incompressible lubrication are also valid for compressible lubrication, at least approximately. Mitsuya et al.[38] have extended the average flow concept to incorporate slip flow conditions. Almost concurrently, Bhushan and Tonder[39,40] have considered the surface roughness and gas rarefaction by using the flow factors derived for incompressible lubrication[34] and modified local flow rates derived from the first order slip flow model[28].

Since the effects of roughness and rarefaction are coupled, some additional corrections are needed. Li et al.[41] derived the modified Reynolds equation for arbitrary roughness orientation. Their model includes the coupled effects of surface roughness and gas rarefaction. For ultra thin layer, the modified Reynolds equation was extended[42] to include higher order slip flow models[43] and was simplified by dropping the Couette flow term which considers the effect of cross flow. Hwang et al.[43] also proposed the use of Modified Molecular Gas film Lubrication (MMGL) equation along with the coupled effects of surface roughness and gas rarefaction. The inertial effects which become dominant at higher frequencies are also discussed in the lubrication problem[44,45].

Blech[27] and Griffin[26] developed formulae for calculating squeeze film force for rectangular and circular plates. They linearized the governing equation (the Reynolds equation) of the squeeze film flow and then calculated the squeeze film force formula. Their models are applicable to only small amplitude oscillation devices. They also showed that the viscous damping effect of the air film dominates at low frequencies while spring effect dominates at higher frequencies. Their models have been justified experimentally by Turner et al.[17]. However, large amplitude oscillations are also common in several devices such as deformable mirror devices (DMD), pull-in pressure sensors, etc. These devices require a solution of nonlinear Reynolds equation for the calculation of squeeze film force[46]. Some of the issues of nonlinearity in the squeeze film dynamics have been studied by Antunes and Piteau[47], but their work is limited to one-dimensional flows.

Veijola et al.[48] have developed an expression for Poiseuille flow rate based on the data made available by Fukui and Kaneko[33]. Li[49] linearized the MMGL equation to find out squeeze film damping in MEMS structures but under the same slip model used by Wang and Cheng[43].

It is clear from the developments discussed above that the Reynolds equation forms the basis of almost all models. Therefore, we begin our discussion on mathematical modelling by discussing different variants of Reynolds equation derived from the Navier-Stokes equations under different assumptions.

2.2. *Different models derived from Navier-Stokes equations*

The fluid flow in continuum regime is governed by the continuity equation and the Navier Stokes momentum equations which are valid for unsteady, compressible and viscous flow. The equations in terms of 3-D spatial co-ordinates and 1-D temporal co-ordinate are written in concise vector form as

continuity equation:

$$\frac{\partial \rho}{\partial t} + \nabla \cdot (\rho \mathbf{u}) = 0; \tag{7}$$

the Navier-Stokes equation:

$$\rho \left\{ \frac{\partial \mathbf{u}}{\partial t} + (\nabla \mathbf{u})\mathbf{u} \right\} = F - \nabla p + (\mu^* + \mu)\nabla(\nabla \cdot \mathbf{u}) + \mu \nabla \cdot (\nabla \mathbf{u}); \tag{8}$$

where, F represents the body forces and $\mathbf{u} = \mathbf{i}u + \mathbf{j}v + \mathbf{k}w$ the velocity, ρ the density of fluid, μ^* the coefficient of dilatational viscosity, and μ the coefficient of shear viscosity or dynamic viscosity.

Let us consider a flow problem illustrated in Fig. 4, where a rectangular plate oscillates normal to the substrate. For small air-gap separating the two plates the squeeze film flow is predominantly two dimensional (i.e., in the x-y plane). Generally, we can make the following assumptions:

- No external forces act on the film, thus $F = 0$
- The structure oscillates with a small amplitude and the main flow is driven by pressure gradients in the x and y directions. So all the terms with w are small and therefore neglected
- No slip flow occurs at the planar boundaries
- No variation of pressure across the fluid film
- The flow is laminar; no vortex flow and no turbulence occur anywhere in the film
- Fully developed flow is considered within the gap
- Flow is assumed to be isothermal, i.e., $p \propto \rho$.

The Navier-Stokes equations (8) then reduce to:

$$\rho\left(\frac{\partial u}{\partial t} + u\frac{\partial u}{\partial x} + v\frac{\partial u}{\partial y}\right) = -\frac{\partial p}{\partial x} + \frac{\partial}{\partial z}\left(\mu\frac{\partial u}{\partial z}\right)$$

and (9)

$$\rho\left(\frac{\partial v}{\partial t} + u\frac{\partial v}{\partial x} + v\frac{\partial v}{\partial y}\right) = -\frac{\partial p}{\partial y} + \frac{\partial}{\partial z}\left(\mu\frac{\partial v}{\partial z}\right).$$

Furthermore, when the gap is much smaller than the surface dimensions, and velocities u and v are relatively small, the convective inertial terms $u\frac{\partial v}{\partial x}$, $v\frac{\partial v}{\partial y}$, $u\frac{\partial u}{\partial x}$ and $v\frac{\partial u}{\partial y}$ can be ignored[50]. Dropping these terms, we rewrite eq. (8) as

$$\rho\left(\frac{\partial u}{\partial t}\right) = -\frac{\partial p}{\partial x} + \frac{\partial}{\partial z}\left(\mu\frac{\partial u}{\partial z}\right)$$

and (10)

$$\rho\left(\frac{\partial v}{\partial t}\right) = -\frac{\partial p}{\partial y} + \frac{\partial}{\partial z}\left(\mu\frac{\partial v}{\partial z}\right)$$

If we also neglect the unsteady inertial terms, eq. (10) reduce to

$$\frac{\partial p}{\partial x} = \frac{\partial}{\partial z}\left(\mu\frac{\partial u}{\partial z}\right)$$

and (11)

$$\frac{\partial p}{\partial y} = \frac{\partial}{\partial z}\left(\mu\frac{\partial v}{\partial z}\right)$$

Using these equations, along with the continuity equation, the generalized Reynolds equation is derived as follows. Equations (10) are first solved for u and v under no slip (i.e., $u|_{\pm h/2} = 0$ and $v|_{\pm h/2} = 0$) boundary conditions.

$$u = \frac{1}{2\mu}\frac{\partial p}{\partial x}\left(z^2 - \frac{h^2}{4}\right)$$

and (12)

$$v = \frac{1}{2\mu}\frac{\partial p}{\partial y}\left(z^2 - \frac{h^2}{4}\right).$$

The average radial velocities $\tilde{u}$ and $\tilde{v}$ are then obtained by integrating equation (12) over the air-gap height as

$$\tilde{u} = -\frac{h^2}{12\mu}\frac{\partial p}{\partial x} \quad \text{and} \quad \tilde{v} = -\frac{h^2}{12\mu}\frac{\partial p}{\partial y}. \tag{13}$$

We now integrate the continuity equation (7) across the gap from $-h/2$ to $+h/2$ as

$$h\frac{\partial \rho}{\partial t} + \frac{\partial}{\partial x}\left[\rho\int_{-h/2}^{h/2} u\,dz\right] + \frac{\partial}{\partial y}\left[\rho\int_{-h/2}^{h/2} v\,dz\right] + \rho\frac{\partial h}{\partial t} = 0. \tag{14}$$

Note that we have made a substitution for the velocity in z direction, $w = \frac{\partial h}{\partial t}$. The integrals above represent average velocities multiplied by h and can be replaced with $\tilde{u}h$ and $\tilde{v}h$. Furthermore, we assume the flow to be isothermal, i.e., $p \propto \rho$ and get the ***nonlinear compressible Reynolds equation:***

$$\frac{\partial}{\partial x}\left(\frac{ph^3}{\mu}\frac{\partial p}{\partial x}\right) + \frac{\partial}{\partial y}\left(\frac{ph^3}{\mu}\frac{\partial p}{\partial y}\right) = 12\frac{\partial(ph)}{\partial t}. \tag{15}$$

In the next subsections, we discuss two important modifications to this equation, viz., to account for the rarefaction effects and the inertial effects.

2.2.1. *Rarefaction considerations*

For very small values of Knudsen number Kn, the first order slip boundary conditions $u|_{\pm h/2} = \mp\lambda\frac{\partial u}{\partial z}$ and $v|_{\pm h/2} = \mp\lambda\frac{\partial v}{\partial z}$ are applied and the slip-corrected velocity distributions can be obtained from equations (9) as

$$u = \frac{1}{2\mu}\frac{\partial p}{\partial x}\left(z^2 - \frac{h^2}{4} - \mathrm{Kn}h^2\right)$$

and (16)

$$v = \frac{1}{2\mu}\frac{\partial p}{\partial x}\left(z^2 - \frac{h^2}{4} - \mathrm{Kn}h^2\right).$$

Figure 7: Perforation geometries: (A) Condenser microphone: close-up of a thin perforated back-plate, the underlying membrane and the air-gap in between (A. Kovacs et al., JMM, 5, 1995) suitably modelled as a 2-D flow case, (B) Tuning fork gyroscope: close up of a high aspect ratio perforated proof mass, the underlying substrate and the air-gap in between; (Kwok et al. JMEMS, 14(4) 2005) best modelled as a 3-D flow case.

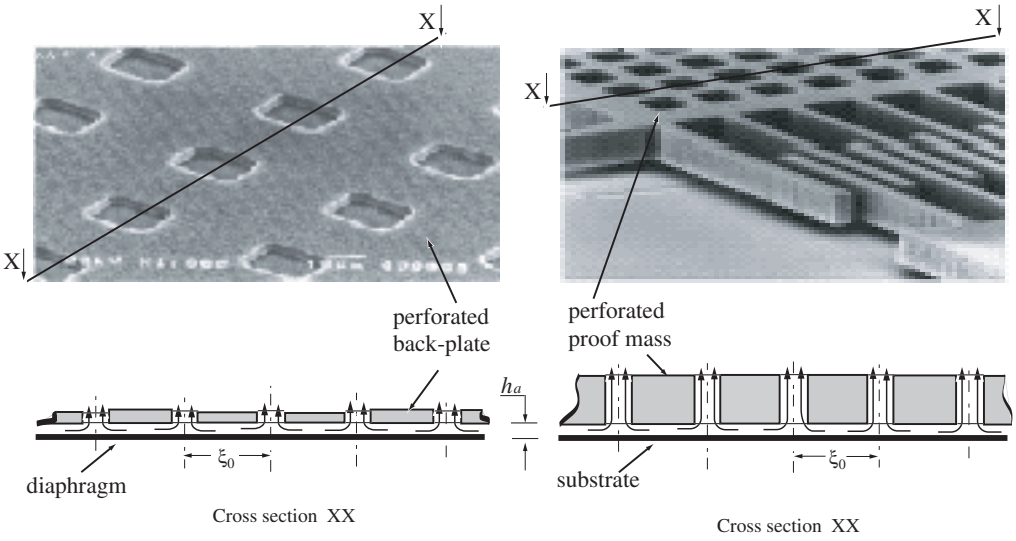

(A) Squeeze-film flow in x-y plane, the flow is predominantly planar i.e., 2-D .

(B) Squeeze-film flow in x-y plane and through the perforations along z-axis, 3-D flow.

We obtain the average radial velocity $\tilde{u}$ and $\tilde{v}$ as

$$\tilde{u} = -\frac{h^2(1+6\mathrm{Kn})}{12\mu}\frac{\partial p}{\partial x} \quad \text{and} \quad \tilde{v} = -\frac{h^2(1+6\mathrm{Kn})}{12\mu}\frac{\partial p}{\partial y}; \tag{17}$$

and substituting these in the continuity equation we obtain the ***nonlinear compressible Reynolds equation with slip* correction:**

$$\frac{\partial}{\partial x}\left(\frac{ph^3(1+6\mathrm{Kn})}{12\mu}\frac{\partial p}{\partial x}\right) + \frac{\partial}{\partial y}\left(\frac{ph^3(1+6\mathrm{Kn})}{12\mu}\frac{\partial p}{\partial y}\right) = \frac{\partial(ph)}{\partial t}. \tag{18}$$

The relative flow rate coefficient, Q_{pr}: when incorporated in the ordinary Reynolds equation, enables modelling the effects of rarefaction and/or inertia.

The factor $(1+6\mathrm{Kn})$ in the above equation is referred to as the relative flow rate coefficient $Q_{\mathrm{pr}} = (1+6\mathrm{Kn})$. The relative flow rate coefficient is generally included in the fluid viscosity and the combined term is called the effective viscosity, $\mu_{\mathrm{eff}} = \frac{\mu}{Q_{\mathrm{pr}}}$. Veijola et al.[51] present a simple approximation for the effective viscosity by fitting the respective flow rate coefficients to the experimental values tabulated by Fukui and Kaneko[32]. This relationship is given as $\mu_{\mathrm{eff}} = \frac{\mu}{1+9.638\mathrm{Kn}^{1.159}}$. There are also many other analytical models to consider rarefaction which are compared with the experimental results later in subsection 4.2.1.

2.2.2. *Inertial effects*

A modified Reynolds equation[50] is derived from equations (9) which include the unsteady inertial terms. Thus, including inertial effects and slip correction, the velocity profiles for small amplitude harmonic excitation (i.e., $\hat{h} = \delta e^{j\omega t}$) are obtained as

$$u = \frac{1}{j\omega\rho}\left(\frac{\cos(qz)}{\cos(qh/2) - \lambda q \sin(qh/2)} - 1\right)\frac{\partial p}{\partial x}, \quad v = \frac{1}{j\omega\rho}\left(\frac{\cos(qz)}{\cos(qh/2) - \lambda q \sin(qh/2)} - 1\right)\frac{\partial p}{\partial y}, \tag{19}$$

where $q = \sqrt{j\omega\rho/\mu}$. Following the same procedure as before, i.e., substituting the average velocities in the continuity equation we get ***compressible Reynolds equation with inertia and slip correction:***

$$\frac{\partial}{\partial x}\left(\frac{ph^3}{\mu}Q_{\mathrm{pr}}\frac{\partial p}{\partial x}\right) + \frac{\partial}{\partial y}\left(\frac{ph^3}{\mu}Q_{\mathrm{pr}}\frac{\partial p}{\partial y}\right) = \frac{\partial(ph)}{\partial t}. \tag{20}$$

Here, the value of Q_{pr} with the inertial effects and the gas rarefaction effects, based on the first order slip, turns out to be $Q_{pr} = \frac{12}{-j\mathrm{Re}} \frac{[(2-\lambda j\mathrm{Re})\tan(\sqrt{-j\mathrm{Re}}/2)-\sqrt{-j\mathrm{Re}}]}{[\sqrt{-j\mathrm{Re}}(1-\lambda\sqrt{-j\mathrm{Re}}\tan(\sqrt{-j\mathrm{Re}}/2))]}$ where $\mathrm{Re} = \frac{\rho\omega h_a^2}{\mu}$ $(= qh)$ is the Reynolds number. Figure 5 shows the frequency response of a square plate obtained by Veijola[50] using eq. (19). It is seen that besides viscous forces that dominate at small frequencies, gas compressibility and inertial forces determine the amount of net force at higher frequencies.

Reynolds number, Re: is the ratio of inertial force to the viscous force.

Squeeze number, σ: is the measure of compressibility of gas. Low squeeze numbers mean gas escapes readily; high values indicate gas is trapped between the structures due to its viscosity.

3. Squeeze film damping in MEMS devices

For many MEMS structures having small amplitude oscillations, the assumption of a rigid structure simplifies the model to a one degree of freedom spring-mass-damper. This assumption leads to analytical solutions when the linearization is applied to the Reynolds equation.

3.1. *Small amplitude approximations*

For small amplitude displacement of the plate, the compressible Reynolds equation (15) can be linearized using the perturbation parameters $\hat{p}$ (in pressure) and $\hat{h}$ (in gap), which were first introduced by Griffin[26]. We substitute $p = P_a + \hat{p}$ and $h = (h_a + \hat{h})$ and neglect the higher order terms to get the following ***linearized compressible Reynolds equation:***

$$\left[\frac{\partial^2\hat{p}}{\partial x^2} + \frac{\partial^2\hat{p}}{\partial y^2}\right] = \frac{12\mu}{P_a h_a^3}\left[h_a\frac{\partial\hat{p}}{\partial t} + P_a\frac{\partial\hat{h}}{\partial t}\right]. \quad (21)$$

For convenience, we will drop the hat in $\hat{p}$ and $\hat{h}$ from here onwards with an implicit understanding that we are working with perturbation variables p and h about the reference pressure P_a and equilibrium gap h_a, respectively. Further, if air is assumed to be incompressible (i.e., $\frac{\partial p}{\partial t} = 0$), eq. (21) can be reduced to the form known as the ***incompressible Reynolds equation:***

$$\frac{\partial^2 p}{\partial x^2} + \frac{\partial^2 p}{\partial y^2} = \frac{12\mu}{h^3}\frac{\partial h}{\partial t}. \quad (22)$$

3.2. *Analytical solution*

Equation (21) can be non-dimensionalized using new variables $\Phi = \frac{\hat{p}}{P_a}$, $\epsilon = \frac{\hat{h}}{h_a}$, $\tau = \omega t$, $X = x/L$, $Y = y/L$, where $\omega =$ the circular frequency and $L =$ the side of a square plate. In terms of these variables, eq. (21) can be written as

$$\left[\frac{\partial^2\Phi}{\partial X^2} + \frac{\partial^2\Phi}{\partial Y^2}\right] = \sigma\left[\frac{\partial\Phi}{\partial\tau} + \frac{\partial\epsilon}{\partial\tau}\right] \quad (23)$$

where $\sigma = \frac{12\mu L^2\omega}{P_a h_a^2}$, is called the squeeze number which measures the compressibility of the fluid. Its significance is discussed in details in subsection 4.2.2.

Analytical solutions for squeeze film damping are reported for transverse and tilting motions in case of simple geometries such as rectangular plates, circular plates and annular plates, etc[26]. As early as 1917, analytical expressions for estimating the stiffness and the damping offered by the air film between two circular plates for condenser transmitters were given by Crandall[52]. For rigidly oscillating rectangular plate, Blech[27] solved the linearized Reynolds equation with ambient pressure at the boundaries and presented a closed form solution for the damping and spring coefficients as:

$$c_a = \frac{64\sigma P_a\chi W^2}{\pi^6\omega h_a} \times \sum_{m,n,odd}\frac{m^2\chi^2+n^2}{(mn)^2\{[m^2\chi^2+n^2]^2+\sigma^2/\pi^4\}} \quad (24)$$

$$k_a = \frac{64\sigma^2 P_a\chi W^2}{\pi^8 h_a} \times \sum_{m,n,odd}\frac{1}{(mn)^2\{[m^2\chi^2+n^2]^2+\sigma^2/\pi^4\}} \quad (25)$$

where $\chi = L/W$ is the length to width ratio of the rectangular plate, P_a is the ambient pressure, h_a is the air gap height and ω is the frequency of oscillations of the plate. The central parameter in these expressions is the squeeze number σ, given by $\sigma = \frac{12\mu L^2\omega}{P_a h_a^2}$ which is a measure of the compressibility. The compressibility is proportional to the square of the lateral dimension to air-gap ratio $(\frac{L}{h_a})$ and the frequency of oscillation (ω), and inversely proportional to the ambient pressure (P_a). The variation of damping and spring forces with squeeze number, plotted as a function of frequency of oscillation $\sigma_{(\omega)}$, is shown in Fig. 6. Initially, the damping force increases steadily with frequency, reaches a maximum value and thereafter decreases monotonically. At low frequencies the air can escape easily however, with increase in frequency of oscillation the fluid compression begins to dominate over the fluid flow and the spring force gradually increases and reaches a maximum value. The point of intersection of the two curves is known as the cut-off frequency. Similar analysis is reported for circular and annular plates and for the torsional motion of plates as well[26]. Torsional motions are encountered in MEMS torsional mirrors.

These formulae are found to be useful for estimating squeeze film effects in simple MEMS

Figure 8: Pressure contours around the perforations (for air gap $= 1\mu$m, frequency $f = 10kHz$) : (A) staggered hole configuration; (B) non-staggered (matrix) hole configuration[54].

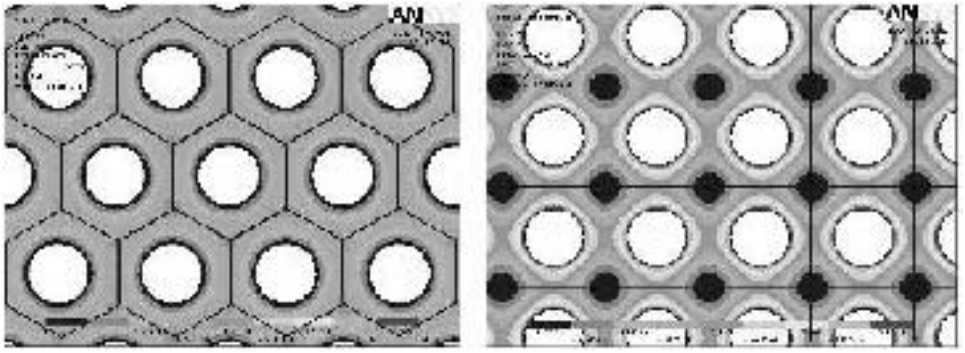

(A) (B)

structures. However, many MEMS structures have very intricate etch hole topography as shown in Fig. 7 and the complexity in analysis increases many folds when one considers associated fluid flow calculations for damping. Moreover, many other effects such as rarefaction, compressibility and even inertia may come into play under different operating frequencies. Different approaches have been reported over a decade. In the next section, we briefly review various models that deal with these issues.

4. Complexities

The problem of squeeze film damping in MEMS transducers becomes more involved because of the complexities arising from inclusion of perforations, shrinking length scales and relatively high frequencies of operation. On one hand, scaling down the dimensions makes the validity of continuum assumption questionable and requires careful modelling, on the other hand, conflicting demands on damping arise while designing for desired dynamic characteristics such as the natural frequency and Q-factor along with the electromechanical sensitivities.

At this stage it will be important to understand the complex relationship of device geometry with the squeeze film damping phenomenon and critical performance parameters of the device. Let us consider a simple device with two parallel plates, one free to vibrate transversely and the other fixed (as a substrate). If we consider this device to be a capacitive sensor or actuator, the most common case in dynamical MEMS devices, a reasonable design goal will be to maximize the compliance ($C_m \propto \frac{A}{t^3}$) for higher mechanical sensitivity and have a high base capacitance ($C_b \propto \frac{A}{h_a}$) for better electrical sensitivity. This clearly requires sufficiently high surface area (A) and small thickness (t) of the vibrating structure, and a very small air-gap (h_a) separating the two structures. However, the air in the small gap between the transversely moving planar structure and the fixed substrate imparts damping, spring and inertial forces to the structures[17,50]. These forces have a complex dependence on the air-gap height and the operating frequency. This affects the frequency response of the structure and hence the sensitivity, resolution and the bandwidth of the device. The damping due to the squeeze film is considerably high for large surface to air-gap ratio ($\propto \frac{A}{h_a^3}$). At low frequencies, damping dominates whereas at high frequencies spring and inertial effects dominate.

The damping can be minimized if it is possible to operate the device under vacuum condition which, in turn, requires an expensive packaging. However, in most cases, the Q-factor of a vibrating system is still mainly determined by the energy losses to the surrounding air as the vacuum in the encapsulated device can hardly be high enough[53]. The amount of the squeeze film damping can be controlled by providing perforations to one of the planar structures, namely, the back plate or the oscillating proof mass. These perforations also facilitate the etch release of the sacrificial layer in surface micromachining but reduce the device capacitance which is undesirable. Adequate value of the base capacitance can be obtained by having smaller air-gap spacing. While reducing the air gap, the perforations need to be designed such that a constant damping is maintained without sacrificing the capacitance. A feasible range of perforation geometry depends on the chosen micromachining process. To achieve the design

Figure 9: Schematic showing: (A) staggered hole configuration: hexagonal pattern (A-B-C-D-E-F) and circular pressure cells within it; (B) non-staggered (matrix) hole configuration: square pattern (L-M-N-O).

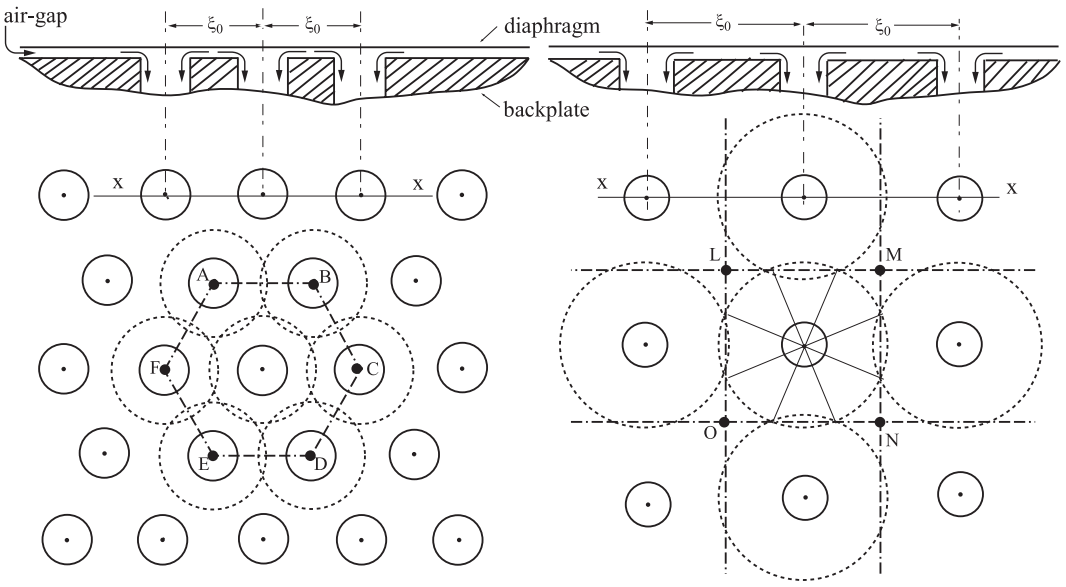

(A) Staggered hole configuration

(B) Non-staggered hole configuration

goals of minimizing damping and maximizing the capacitance a trade-off analysis has to be carried out between the perforation geometry and the air-gap. This necessitates creation of simple analytical models and derivation of closed-form formulae for the squeeze film analysis. These in turn should be validated using FEM tools or experimental measurements. The forces due to the squeeze film extracted from these behavioural models are in turn employed in a system-level model for the performance optimization of a MEMS device. Thus, the air-gap h_a, is perhaps the single most crucial parameter which affects the squeeze film behaviour, base capacitance and hence the overall device performance. Clearly, efficient models for the squeeze film analysis of MEMS structures are indispensable in the design of MEMS devices.

4.1. ***Modelling strategies for perforated structures***

The squeeze film flow in dynamic MEMS structures is modelled well by the 2D Reynolds equation obtained from the Navier-Stokes equation by neglecting inertia and assuming the lateral dimension to be an order of magnitude larger than the air-gap height. Figure 8 shows typical pressure contours plotted over the fluid domain for commonly encountered staggered and non staggered configurations of perforations. It is observed that in both configurations of the holes there is order and symmetry in the pressure contours. Various approaches based on analytical, numerical and mixed techniques are found in literature which model perforated structure. The analytical approaches employ following two strategies:

1. Pressure cell concept: The inherent symmetry in the distribution of holes leads to the formation of repetitive pressure patterns around each hole in the entire fluid domain. This particular fact is exploited in this approach by analysing the problem for a single hole embedded in a single 'cell', and then obtaining the result for the entire structure by multiplying with the number of cells (see Fig. 9).
2. Modified Reynolds equation: In this approach, the Reynolds equation is modified to include the flow leakage at the perforations.

For perforated MEMS structures, the effective lateral dimension is the pitch of the holes (ξ_o). Therefore, in the case of perforated structures the assumption of large lateral dimension begins to deviate. Moreover, the flow through the perforations comes into play adding an extra dimension to the model. The model dimensionality (2D, or 3D) is governed by the relative size of the perforation parameters. The significant perforation parameters are the pitch (ξ_o), the diameter (d), and the length of the holes (l, which is the same as the thickness of the perforated plate). Various models have been

Figure 10: An overview of the existing squeeze film models for perforated structures (ξ_o is the pitch of the holes, h_a is the air-gap height, l and d are length and diameter of the holes, respectively).

Different perforation geometries and modelling methodologies			**Important effects modelled**			**Solution methods**
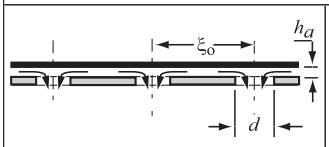 (a) Lateral flow - 2D model	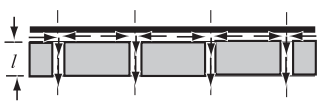 (b) Two discrete flows Lateral flow-2D / vertical flow-1D	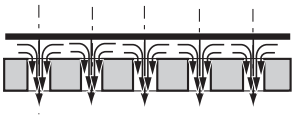 (c) Full 3D flow model $\xi_o \sim h_a \sim l \sim d$	Rarefaction effects: Effective viscosity, Slip-flow boundary	Compressibility effects	Inertial effects	Analytical (A), Numerical(N)
$\frac{\xi_o}{h_a}$ ⟶ high (>20)	moderate (10 - 20)	low (< 10)				
$\frac{l}{d}$ ⟶ low (< 1)	high (> 1)	moderate (~ 1)				
$\frac{r_i}{h_a}$ ⟶ high (> 5)	moderate (1-5)	low (~ 1)				
Starr [67] Reynolds Eq. solved, for large air-gap/ incompressible flow.			✗	✗	✗	N
Chen et al. [71]; Nonlinear Reynolds Eq. venting boundary condition (P = 0).			✓	✗	✗	N
Yang et al. [46]; Nonlinear Reynolds Eq. used for flexible microstructure with large amplitude motions.			✗	✓	✗	N
M. G. da Silva et al. [73]; A hybrid model using Reynolds Eq. for the air-gap and the Navier–Stokes Eq. near all edges and perforations is developed. Navier–Stokes–Reynolds (NSR) solver.			✓	✓	✗	N
Schrag et al. [74, 75], Sattler et al. [76]; Mixed level model, accounts for finite size effect and non-developed flows, uses Finite Network (FN) model of Reynolds Eq., and compact models for edge effect and perforations (implemented in VHDL-AMS).			✓	✓	✗	N
Råback et al. [77] ; Hierarchical model, first the flow through holes is simulated numerically and homoginized uniformly on the damper surface in the modified Reynolds equation.			✓	✗	✗	N
Veijola et al. [72] ; Reynolds Eq. modified by adding "leakage" flow through perforations, described as a spatially variable perforation profile, implemented in Perforation Profile Reynolds (PPR) solver.			✓	✓	✗	N
Skvor [55]; Incompressible flow trivial venting boundary condition (P = 0).			✗	✗	✗	A
Veijola et al. [60]; Reynolds Eq. modified by augmenting the flow impedance due to perforationns (homogenization approach).			✓	✗	✗	A
Bao et al. [58,59]; Reynolds Eq. modified by adding a term related to damping effect of gas flow through holes based on Poiseuille Eq., flow resistance at entry/exit of holes neglected.			✗	✗	✗	A
Homentcovschi et al. [56,57]; Reynolds Eq. modified to include inertia, trivial venting boundary condition (P = 0) used.			[56] ✗ [57] ✓	[56] ✗ [57] ✓	[56] ✓ [57] ✓	A
Mohite et al. [54]; Compressibe Reynolds Eq. solved, trivial venting boundary condition (P = 0) used.			✓	✓	✗	A
Darling et al. [61], Reynolds Eq. solved, nontrivial venting condition based on the acoustical impedence of aperture is used.			✗	✗	✗	A
Kwok et al. [62]; Reynolds Eq. is used and the boundary condition on holes is derived using pipe flow analysis (incompressible), loss due to gas flow through holes added.			✓	✗	✗	A
Veijola [63]; Used existing analytical models for squeeze-film (Skvor) and capillary (pipe flow) regions, and derived flow resistances for the intermediate region and out flow by FEM simulations for incompressible flow.			✓	✗	✗	A

Figure 11: Simulated dynamical response of the microaccelerometer with and without air film damping effects (Yang et al. Proc. IEEE Solid State Sensors and Actuators Workshop, SC, USA 1996).

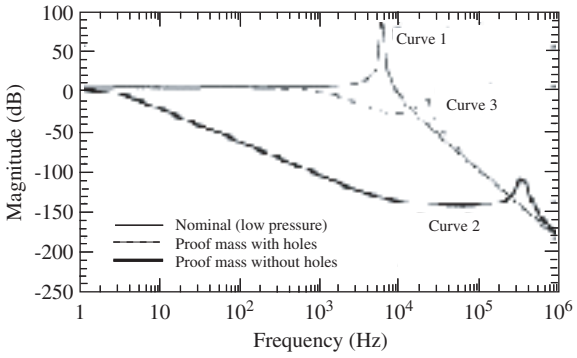

presented for the squeeze film analysis of perforated MEMS structures in the literature spanning over a decade. These models differ from each other in the way they treat the flow (e.g., 2D, or 3D), and the effects they include in the analysis (e.g., rarefaction, compressibility and inertia etc.). Figure 10 gives an overview of different squeeze film models at a glance. We now discuss some analytical models used for various perforation geometries.

When the size of the holes is much larger compared to the air-gap height ($d > 10h_a$) and the perforations are short ($l < d$) as shown in figure 10(a), the loss through the holes is not significant. In this case, the problem is reduced to solving the 2-D Reynolds equation under the simplified boundary condition that the acoustic pressure vanishes at the edge of a hole. Closed-form solutions derived assuming incompressible flow exist for such geometries[55]. This is based on the concept of pressure cell mentioned above. The damping coefficient R_a for a square plate of side length L having perforation density n is given by

$$R_a = \frac{12\mu L^2}{nh_a^3\pi}\left(\frac{\alpha}{2} - \frac{\alpha^2}{8} - \frac{\ln(\alpha)}{4} - \frac{3}{8}\right), \qquad (26)$$

where α is the perforation fraction. Solutions including rarefaction, compressibility and inertial effects are also reported for such geometries[54,56–58].

Deep Reactive Ion Etching (DRIE): is a highly anisotropic etch process developed for MEMS and used to create high aspect ratio holes and trenches in silicon.

For inertial MEMS sensors (e.g., gyroscope, accelerometer, etc.), high aspect ratio perforated structures using deep reactive ion etching (DRIE) process are used as shown in figure 10(b). In this case, the loss through the holes can be significant as the flow is a combination of the horizontal flow between the planar surfaces and the vertical flow through the holes. Bao et al.[59,60] have modelled this problem by modifying the Reynolds equation using a pressure leakage term corresponding to the loss through the holes (in the z direction). The modified incompressible Reynolds equation based on this model is given as

$$\frac{\partial^2 p}{\partial x^2} + \frac{\partial^2 p}{\partial y^2} - \underbrace{\frac{3\beta^2 r_o^2}{2h^3 H}\frac{1}{\eta(\beta)}p}_{\text{pressure leakage term}} = \frac{12\mu}{h^3}\frac{\partial h}{\partial t}. \qquad (27)$$

This model is suitable for the uniformly distributed holes where the loss through the holes is homogenized over the entire domain. For arbitrary perforation having complex shapes, and nonuniform distribution and size, Veijola et al.[61] have suggested another model. This model utilizes a Perforation Profile Reynolds solver (PPR: a multiphysics simulation software), which includes additional terms in the modified Reynolds equation that model the leakage flow through the perforations, and variable viscosity and compressibility profiles. The frequency domain form of the equation is given as

$$\nabla \cdot \left(\frac{D_h h^3 Q_{pr}}{12\mu}\nabla p\right) - C_h \frac{j\omega h}{P_a} p - Y_h p = w; \quad (28)$$

where $D_h(x, y)$, $C_h(x, y)$ and $Y_h(x, y)$ are extentions that are specific for perforated structures: relative diffusivity, relative compressibility, and perforation admittance profiles, respectively. Wider perforation geometries can be treated with this model, however, it requires special computational tools and takes time to build the model.

Alternatively, the flow problem can be treated in two distinct parts. The damping effect due to the lateral flow is modelled by Reynolds equation and the flow through the holes is modelled by Poiseuille equation. However, in the region just above the hole where the lateral squeeze flow joins the poiseuille flow, there is a complex interaction causing losses which are difficult to estimate. Moreover, the trivial boundary condition that the acoustic pressure vanishes at the edge of a hole does not hold. Darling et al.[62] used arbitrary pressure boundary conditions based on complex acoustical impedance of an aperture and treated the squeeze film problem using Green's function approach. Kwok et al.[63] used the boundary condition on the hole evaluated for incompressible flow in the numerical simulation performed using PDEase, a custom made finite element solver. Under the assumption of incompressible flow (i.e., low squeeze number), the flow through a hole is obtained merely by geometrical scaling between the cell diameter to the hole diameter. In a recent study,

Figure 12: The damping, spring and inertial nature exhibited by air at different values of the squeeze number σ and the Reynolds number Re; (A) squeeze film is predominantly viscous, (B) squeeze film is viscous and compressible, (C) squeeze film besides being viscous and compressible, exerts inertia

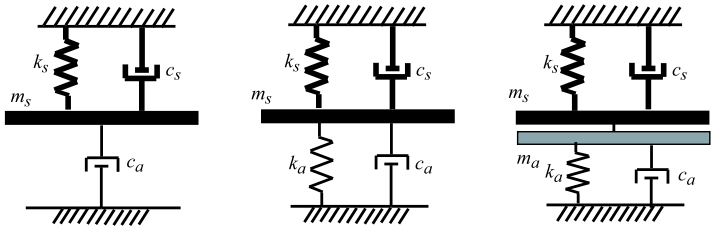

(A) $\sigma < 1$, $\mathrm{Re} < 1$ (B) $\sigma > 1$, $\mathrm{Re} < 1$ (C) $\sigma > 1$, $\mathrm{Re} > 1$

Veijola[64] used existing analytic models in the squeeze film and capillary regions, and using FEM simulations derived approximate flow resistances at the intermediate region and at the exit flow from the hole. The model is valid over a wide range of perforation fractions (1% to 90%). The study also presents analysis of cut-off frequencies for compressibility and inertia and specifies an upper limit on the frequency up to which the model is valid.

When the pitch of the holes, the air-gap and the diameter of the holes are all of the same order as shown in figure 10(c), the assumptions made in deriving the Reynolds equation do not hold and the computationally intensive 3D Navier-Stokes analysis becomes indispensable. In a recent study, a surface extension model is proposed[65], where the gap size is comparable to the lateral dimensions. In this approach it is shown that after extending each open border by $(1.3/2)h_a$ the 2D Reynolds equation can give accurate results and 3D Navier-Stokes equation can be dispensed with. This approach could be applied to the perforated structures as well.

4.2. *Criteria for considering Rarefaction, Compressibility and Inertia*

In this section, we discuss various phenomena associated with the squeeze film analysis in terms of some non-dimensional numbers characterizing them and highlight how they are related to the perforation geometry and the operating frequency of a device.

4.2.1. *Rarefaction*

In the presence of perforations, we have to worry about rarefaction effects in two places— the usual horizontal expanse between the vibrating plate and the fixed plate, and the airflow space in the holes. Therefore, we use two Knudsen numbers $\mathrm{Kn_g}$ and $\mathrm{Kn_h}$, for the usual air-gap and the hole, respectively. We define $\mathrm{Kn_g} = \lambda/h_a$, where h_a is the air gap thickness and λ is the mean free path of the gas molecules. Similarly, Knudsen number for the flow through a hole is defined as $\mathrm{Kn_h} = \lambda/r_i$, where r_i is radius of the hole. The parameter λ is related to the packaging pressure P_a as $\lambda = \frac{P_o \lambda_o}{P_a}$. At ambient conditions, the mean free path λ_o for air is 0.064μm. For MEMS devices having very small air-gap and low packaging pressure, the Knudsen number Kn increases and the fluid flow transits from continuum flow to rarified flow. Based on the values of Kn, the flow regimes can be divided into four different types as shown in Table 1[66]. Thus, it is possible to have different flow regimes in the air-gap and the holes. As discussed in section 2.2.1, this effect can be modelled by changing the effective viscosity through the use of corresponding flow factor. Depending on the value of Kn, the value of μ_{eff} and hence the squeeze film damping can vary considerably. For example, the value of damping drops by 30% for 1μm air-gap at 1 atm pressure if slip flow is considered. For the rarefied flow regime, analytical model is derived using the slip-flow wall boundary conditions at the planar surfaces in the air-gap and on the cylindrical wall of the hole. Under normal conditions, the continuum model is used to model gas flow. But under the condition of extremely low density (or extremely small flow length), discrete particle effects become significant, and then we have to adopt discrete model, i.e., the method of rarified gas dynamics[67].

4.2.2. *Compressibility*

The squeeze number σ, which is a measure of the compressibility, is given by $\sigma = \frac{12\mu L^2\omega}{P_a h_0^2}$ (and for perforated structures $\sigma = \frac{12\mu\omega r_o^2}{P_a h_a^2}$ where r_o is the radius of an equivalent circular pressure cell which is approximately half the pitch of the holes ($r_o \approx \xi_o/2$)). Thus, the compressibility is proportional to the square of the lateral dimension to air-gap ratio ($\frac{L}{h_a}$) and the frequency of oscillation (ω), and inversely proportional to the ambient pressure (P_a). If $\sigma \ll 1$ the compressibility can be neglected and the flow is treated as incompressible. For higher values of σ, the compressibility leads to a significant air-spring effect which can be undesirable as it can adversely affect the dynamic behaviour of a device[68]. Contrary to this, the fact that the perforations increase the cut-off frequency, which is the frequency at which the damping and the spring forces are equal, can be exploited by varying the number and size of the perforations[69]. Blech[27] and Allen et al.[70] too have reported the use of squeeze film damping to tailor the frequency

Table 1: Knudsen number Range and the corresponding Flow regimes

Knudsen number (Kn)	Kn < 0.01	0.01 < Kn < 0.1	0.1< Kn <10	Kn > 10
Flow regime	Continuum Flow	Slip Flow	Transitional Flow	Molecular Flow

response of a seismic accelerometer and that of micromachined sensors, respectively. Figure 6 illustrates the simulated small-amplitude dynamical response of a micro-accelerometer fabricated at MIT[46]. Curve 1 is a typical response without any air damping. Curve 2, which rolls off very fast, is the response with air damping indicating the severity of damping at 1μm air-gap. In order to reduce damping, a perforated proof mass was used and the corresponding response is indicated by curve 3 in figure 11. Thus, including the compressibility effects in the analysis enables the designer to design the perforation geometry such that the compressibility effects are either totally ruled out or suitably tuned as the case may be.

4.2.3. *Inertia*

The small dimensions of MEMS devices constitute a very small volume which contains a minuscule quantity of air. Hence, fluid inertia may be neglected at low frequencies ($\mathrm{Re} \ll 1$). However, for larger air-gap height, or at higher frequencies of oscillations the inertial effects may not be negligible. This is done by incorporating the frequency dependent flow rate coefficient Q_{pr} which modifies the velocity profile with frequency[50]. For the squeeze film flow in the air-gap, the modified Reynolds number is defined as $\mathrm{Re_g} = \frac{\rho\omega h_a^2}{\mu}$ and for the flow through the hole it is defined as $\mathrm{Re_h} = \frac{\rho\omega r_i^2}{\mu}$. The Reynolds number in the two cases increases

Figure 13: (A) 2D pressure cell in cylindrical coordinates, (B) 3D pressure cell including loss through the hole, (C) Frequency response (amplitude) of the full 3D squeeze film model including inertia in comparison with the results of 2D model with and without inertia, and numerically simulated model in ANSYS-CFX (×) for $h_a = 4\mu$m, hole size $s = 8\mu$m and $l = 20\mu$m.[71]

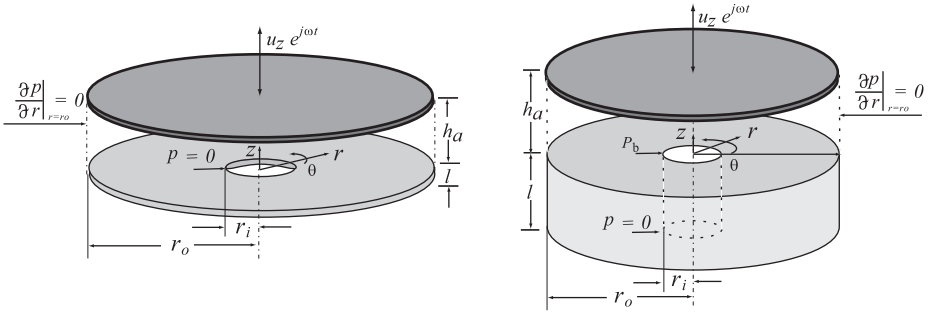

(A) 2D model of a single circular pressure cell (B) 3D model of a single circular pressure cell

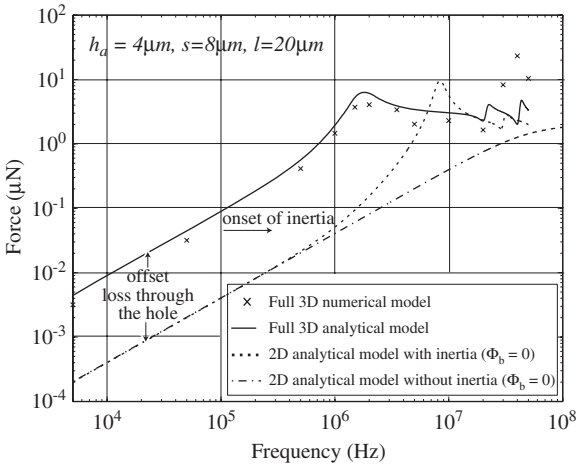

(C) Response curves using analytical and numerical models.

Figure 14: The experimental and theoretical results for the quality factor versus pressure for a torsion mirror given by Minikes et al.[83]

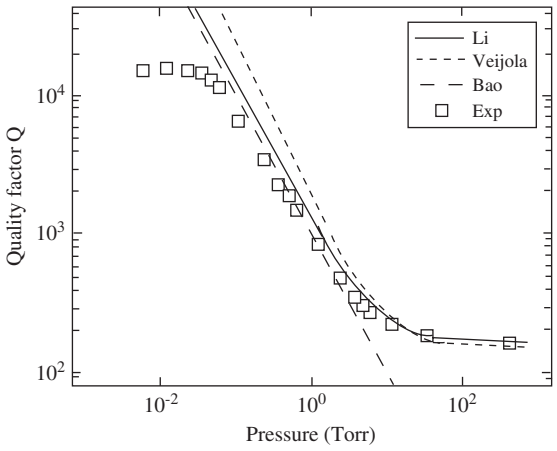

with the square of the air-gap height and the radius of the hole, respectively. Depending on the value of Re, one can ignore or include the inertia of air in the analysis and use appropriate form of equation presented in section 2.2. Fig. 12 shows schematically the incompressible, compressible, and compressible plus inertial nature of squeeze film flow under different values of σ and Re.

4.3. *Numerical solutions and analytical solutions*

Solution methods based on numerical, analytical or mixed techniques are developed to suit different perforation geometries. Numerical methods are best suited for modelling nonlinear pressure response due to high amplitude of oscillation, arbitrary boundary conditions, complex geometries, and nonuniform size and distribution of the holes[68,72,73]. Computationally efficient FEM based simulation schemes are reported in the recent past[73,74]. A hybrid model combining the Navier-Stokes equation and the Reynolds equation is proposed by Da Silva[74]. A mixed level approach based on FEM and finite network (FN) simulation is presented by Schrag et al.[75–77]. A hierarchical two level simulation strategy is employed and coupled, reduced dimensional analysis is performed by Raback et al.[78]. Another method for arbitrary perforation problem utilizes a Perforation Profile Reynolds (PPR) solver, a multiphysics simulation software[73].

The goal of modelling and analyzing squeeze film behaviour in perforated structures is to perform a reasonably accurate analysis with minimal modelling and computational effort. In this respect, analytical methods are desirable since they give closed-form expressions which can be used directly in system-level simulation for evaluating design trade-offs. In these methods, the symmetry of pressure distributions around each hole is exploited and the entire perforated domain is discretized into pressure cells under simplifying assumptions[64,55,63]. However, to set clear limits to these models, extensive and independent numerical simulations are required. For such computations, one often resorts to full 3-D Navier-Stokes solvers available in commercial MEMS packages such as ANSYS-CFX. One such comparative study is shown in figure 13[71]. One can clearly see both quantitative and qualitative changes in response when inertia is considered and when inertia is ignored.

4.4. *Comparison with experimental results*

As mentioned earlier there are basically four important effects—rarefaction effect, compressibility effect, inertial effect, and perforation effect that need to be studied through experiments. The compressibility and inertial effects are dominant only at higher operating frequencies. On the other hand, rarefaction and perforation effects can be seen even at low frequencies.

Rarefaction can be modelled using two approaches. First approach uses the concept of effective viscosity as presented by Veijola et al.[51] and Li et al.[49]. In this case the effective viscosity based on the Knudsen number Kn is used. Second approach is based on the free molecular dynamic models derived for a plate vibrating normal to a fixed substrate. Free molecular models are presented by Christian[79], Zook et al.[80], Kadar et al.[81], Bao et al.[53] and Hutcherson and Ye[82]. Among the first four free molecular models, Bao's model is more accurate and handy. Since Bao's model is valid for only free molecular regime, Hutchersons model can be used for transition regime which is based on molecular dynamic simulations. By comparing all the important analytical models with experimental measurements on a MEMS torsion mirror, Minikes et al.[83] have shown that the effective viscosity model presented by Li et al.[49] are most accurate over different flow regimes as shown in Fig. 14.

Andrews et al.[17] have performed experiments on a silicon microstructure in which fluid damping is due to squeeze film flow. In this study, the experiments are performed for a wide range of pressures ranging from vacuum to atmospheric and over very low to as high as 50 kHz frequencies. At frequencies less than 10 kHz, the formula given by Blech[27] gives good agreement while at higher frequencies there is some discrepancies due the inertia effect which is not included in the Blech's formula. Veijola[50] has proposed an analytical formula for inertial and rarefaction effect which has to be validated with experimental results.

Figure 15: (A) Variation of non-dimensionalized damping and spring force with squeeze number for ϵ = 0.001, 0.05, and 0.1; (B) Percentage change in total non-dimensionalized back force with log(ϵ).

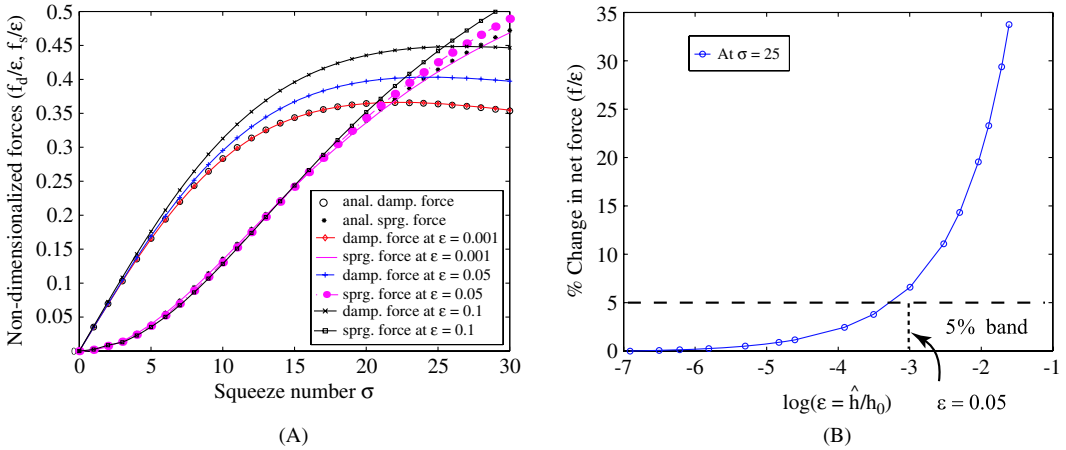

Kim et al.[84] performed experimental studies to estimate viscous damping offered by planar structures having different size and number of perforations. They found that in addition to squeeze film damping, loss through holes and the loss at the boundaries of the suspended structures too are significant. Kowk et al.[63] also performed experiments on perforated MEMS gyroscope to calculate net squeeze film damping and compared it with the analytical results. The formulae given by them is valid for large perforations only. There are various other analytical formulae available as given in Fig. 10 which model perforation and rarefaction effects simultaneously. All of them need to be compared with experimental results for different perforation topologies.

5. Open issues and current thrust

5.1. *Nonlinearities*

The analytical models available in the literatures are derived under the assumptions of small variation in air-gap thickness and pressure. When the amplitude of vibration increases, the non-linear terms in the governing equations start dominating. To study the effect of non-linear terms in the Reynolds equation, the non-dimensional damping and spring forces are numerically obtained by solving non-linear Reynolds equation for different values of non-dimensionalized amplitude ϵ (ratio of vibrational amplitude to the air-gap thickness). The results are obtained for different values of squeeze number as shown in Fig. 15[85]. It is found that when the

Figure 16: (A) Effect of isotropic and anisotropic distribution of roughness patterns on squeeze film damping and spring forces; (B) Effect of different roughness amplitudes on damping and spring forces.

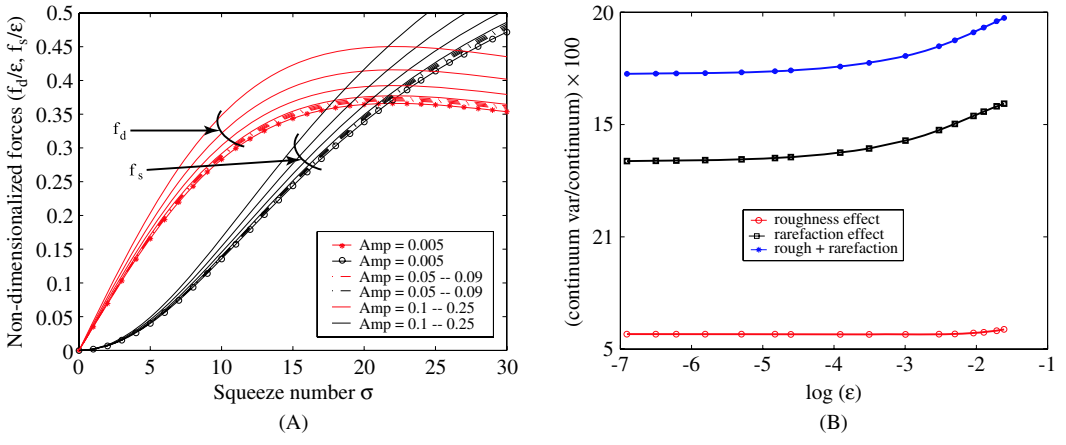

value of ϵ varies from 0 to 20% of the initial gap, the absolute back force increases by more than two orders of magnitude (Fig. 15(B)). Since, some of the MEMS devices such as deformable mirror devices and RF switches, etc., have large amplitude motion, nonlinear effects of squeeze film damping need to be investigated well.

5.2. *Effect of surface roughness*

For most MEMS devices, air-gap thickness is large enough to neglect the effect of surface roughness on squeeze film damping. However, when the size of the device reduces to nano scale the relative amplitude of surface roughness increases and eventually affects the characteristics of squeeze film damper[86]. Theoretical studies show that when the roughness amplitude is about 10% of the air-gap thickness, the surface roughness effect becomes pronounced (Fig. 16(A)). Such condition can be seen in devices with submicron scale air-gap thickness. It is also found that the rarefaction effect obtained by reducing pressure or reducing length scale is also affected by surface roughness as shown in Fig. 16(B). This is because, under rarified gas flow the interaction of gas molecules and irregular surface of the oscillating plate plays an important role in deciding the nature of interaction, i.e., diffusive interaction, specular interaction or a combination of diffusive and specular interactions. Although most of the studies done in the literature use surface roughness of Gaussian distribution, more accurate measurement of surface roughness profile in MEMS structures are needed for reliable modelling. The most challenging part is to measure the roughness profile of two surfaces facing each other in the air-gap thickness without breaking the structures.

6. Conclusions

Squeeze film damping affects the dynamic performance of most MEMS devices that employ vibrating structures with some gas or other fluid trapped between the vibrating surface and a narrowly separated fixed substrate. The effect of the squeeze film on the dynamics of the structure is found by solving fluid flow equations with appropriate conditions to evaluate the back pressure on the structure which in turn gives damping and spring force components. Several analytical solutions exist that provide very good estimates of damping and spring forces due to the squeeze film under various flow conditions (i.e., 1-D, 2-D and 3-D flow). These solutions are based on the mathematical models (mostly variants of Reynolds equation) that differ in their treatment of rarefaction, compressibility, inertia and flow through perforations. Most models compare well with numerical simulations based on direct solution of fluid flow equations. Some models have been experimentally verified as well. However, more careful and varied experiments are required for verification of existing models as well as for better understanding of squeeze film effects at extremely small scales.

Acknowledgments

This study is partially supported by a grant from the Department of Science and Technology (DST), New Delhi, India.

Received 23 December 2006; revised 15 January 2007.

References

1. H. C. Nathanson, W. E. Newell, R. A. Wickstrom, and J. R. Davis, "The resonant gate transistor," *IEEE Transaction on Electron Devices* **ED-14, No. 3**, pp. 117–133, 1967.
2. [online], "Available: http://www.analogdevices.com" *Analog devices Inc.*
3. T. Juneau and A. P. Pisano, "Micromachined dual axis input axis angular rate sensor," *Tech. Dig. Proc. Solid-State Sensor Actuator Workshop* , pp. 299–302, 1996.
4. S. Vemuri, G. Fedder, and T. Mukherjee, "Low order squeeze film model for simulation of mems devices," *Tech. Proc. 2000 International Conference on Modeling and Simulation of Microsystems* , pp. 205–208, 2000.
5. G. Zhou, F. E. H. Tay, and F. S. Chau, "Macro-modelling of a double-gimbaled electrostatic torsional micromirror," *J. of Micromech and Microengg.* **13**, pp. 532–547, 2003.
6. F. Pan, J. Kubby, A. Tran, and S. Mukherjee, "Squeeze film damping effect on the dynamic response of a mems torsion mirror," *J. of Micromech. and Microengg.* **8**, pp. 200–208, 1998.
7. [online], "Available: http://www.dlp.com" *Texas Instruments Inc.*
8. [online], "Available: http://www.akustica.com" *Akustica Inc.*
9. M. Kurosawa, M. Takahashi, and T. Higuchi, "An ultrasonic xy stage using 10 mhz surface acoustic wave," *Proc. IEEE Ultrason. Symp.* , p. 535538, 1994.
10. H. Hosaka, K. Itao, and S. Kuroda, "Damping characteristics of beam-shaped micro-oscillators," *Sensors and Actuators A* **49**, pp. 87–95, 1995.
11. A. H. Nayfeh and M. I. Younis, "A new approach to the modeling and simulation of flexible microstructures under the effect of squeeze-film damping," *J. of Micromech and Microengg.* **14**, pp. 170–181, 2004.
12. C. Zhang, G. Xu, and Q. Jiang, "Characterization of the squeeze film damping effect on the quality factor of a microbeam resonator," *J. of Micromech and Microengg.* **14**, pp. 1302–1306, 2004.
13. M. Paz, *Structural Dynamics: Theory and Computation*, CBS, New Delhi, 1987.
14. R. W. Clough and J. Penzien, *Dynamics of Structures*, McGraw-Hill Inc,NewYork, 1993.
15. R. Lifshiz and M. L. Roukes, "Thermoelastic damping in micro- and nanomechanical systems," *Physical Review B* **61**(8), pp. 5600–5609, 1995.
16. Z. Hao, A. Erbil, and F. Ayazi, "An analytical model for support loss in micromachined beam resonators with in-plane flexural vibrations," *Sensors and Actuators A* **109**, pp. 156–164, 2003.
17. M. Andrews, I. Harris, and G. Turner, "A comparison of squeeze film theory with measurements on a microstructure," *Sensors and Actuators A* **36**(2), pp. 79–87, 1993.
18. J. Yang, T. Ono, and M. Esashi, "Energy dissipation in submicrometer thick single-crystal silicon cantilevers," *IEEE Journal of MEMS* **11**, pp. 775–783, 2002.

19. W. E. Newell, "Miniaturization of tuning forks," *Science* **161**(3848), pp. 1320–1326, 27 Sept. 1968.
20. A. K. Pandey, "Analysis of squeeze-film damping in microdevices," Master's thesis, Department of Mechanical Engineering, Indian Institute of Science, Bangalore-560012, INDIA., November 2003.
21. S. Senturia, *Microsystem Design*, Kluwer Academic Publishers, Boston, 2001.
22. M. H. Bao, *Micro Mechanical Transducers: Pressure Sensors, Accelerometer and Gyroscopes*, Elsevier B. V., The Netherlands, 2000.
23. O. Pinkus and B. Sternlicht, *Theory of Hydrodynamic Lubrication*, McGraw-Hill Book Company, Inc., New York, 1961.
24. W. A. Gross, *Gas Film Lubrication*, John Wiley and Sons, Inc., New York, 1962.
25. W. E. Langlois, "Isothermal squeeze films," *Quarterly Applied Mathematics* **20**(2), pp. 131–150, 1962.
26. W. S. Griffin, H. H. Richardsen, and S. Yamamami, "A study of fluid squeeze film damping," *Journal of Basic Engineering* , pp. 451–456, 1966.
27. J. J. Blech, "On isothermal squeeze films," *Journal of Lubrication Technology* **105**, pp. 615–620, 1983.
28. A. Burgdorfer, "The infuence of the molecular mean free path on the performance of hydrodynamic gas lubrication bearings," *ASME Journal of Basic Engineering* **81**, pp. 94–100, 1959.
29. Y. T. Hisa and G. A. Domoto, "An experimental investigation of molecular rarefaction effects in gas lubricated bearings," *ASME J. of Lubr. Technol.* **117**, pp. 120–130, 1983.
30. Y. Mitsuya, "Modified reynolds equation for ultra-thin film gas lubrication using 1.5-order slip-flow model and considering surface accomodation coefficients," *ASME J. of Tribology* **115**, pp. 289–294, 1993.
31. R. F. Gans, "Lubrication theory at arbitrary knudsen number," *Journal of Tribology* **107**, pp. 431–433, 1985.
32. S. Fukui and R. Kaneko, "Analysis of ultra-thin gas film lubrication based on linearized boltzmann equation: First report- derivation of a generalized lubrication equation including thermal creep flow," *Journal of Tribology* **110**, pp. 253–262, 1988.
33. S. Fukui and R. Kaneko, "A database for interpolation of poiseuille flow rates for high knudsen number lubrication problems," *Journal of Tribology* **112**, pp. 78–83, 1990.
34. N. Patir and H. S. Cheng, "An average flow model for determining effects of three- dimensional roughness on partial hydrodynamic lubrication," *Journal of Lubrication Technology* **100**, pp. 12–16, 1978.
35. H. G. Elrod, "A general theory for laminar lubrication with reynolds roughness," *Journal of Lubrication Technology* **101**, pp. 8–14, 1979.
36. J. H. Tripp, "Surface roughness effects in hydrodynamics lubrication: The flow factor method," *Journal of Lubrication Technology* **105**, pp. 458–465, 1983.
37. K. Tonder, "The lubrication of unidirectional straited roughness: Consequences for some general theories," *ASME Journal of Tribology* **108**, pp. 167–170, 1986.
38. Y. Mitsuya, T. Ohkubo, and H. Ota, "Averaged reynolds equation extended to gas lubrication possessing surface roughness in slip flow regime: Approximate method and confirmation experiments," *Journal of Tribology* **111**, pp. 495–503, 1989.
39. B. Bhushan and K. Tonder, "Roughness-induced shear- and squeeze-film effects in magnetic recording-part i: Analysis," *Journal of Tribology* **111**, pp. 220–227, 1989.
40. B. Bhushan and K. Tonder, "Roughness-induced shear- and squeeze-film effects in magnetic recording-part ii: Applications," *Journal of Tribology* **111**, pp. 228–237, 1989.
41. W. L. Li, C. L. Weng, and C. C. Hwang, "Effect of roughness orientations on thin film lubrication of magnetic recording system," *Journal of Physics D: Applied Physics* , pp. 1011–1021, 1995.
42. W.-L. Li and C.-I. Weng, "Modified average reynolds equation for ultra-thin gas lubrication considering roughness orientations at arbitrary knudsen numbers," *Wear* **209**, pp. 292–300, 1997.
43. C.-C. Hwang, R.-F. Fung, R.-F. Yang, and W.-L. Li, "A new modified reynolds equation for ultrathin film gas lubrication," *IEEE Transactions on Magnetics* **32**(2), pp. 344–347, 1996.
44. H. Hashimoto and S. Wada, "The effects of fluid inertia forces in parallel circular squeeze film bearings lubricated with pseudoplastic fluids," *ASME J. Tribol.* **108**, p. 282287, 1986.
45. H. Hashimoto, "Viscoelastic squeeze film characteristics with inertia effects between two parallel circular plates under sinusoidal motion," *ASME J. Tribol.* **116**, p. 161166, 1994.
46. Y. J. Yang, M. A. Gretillat, and S. D. Senturia, "Effect of air damping on the dynamics of non-uniform deformations of microstructure," *Transducers 97* (2), pp. 1093–1096, 1997.
47. J. Antunes and P. Piteau, "A nonlinear model for squeeze-film dynamics under axial flow," in *ASME PVPConference, Symposium on Flow-Induced Vibration 2001*, (Atlanta, USA), 2001.
48. T. Veijola, H. Kuisma, and J. Lahdenpera, "The influence of gas-surface interaction on gas-film damping in a silicon accelerometer," *Sensors and Actuators A* **66**, pp. 82–92, 1998.
49. W.-L. Li, "Analytical modelling of ultra-thin gas squeeze film," *Nanotechnology* **10**, pp. 440–446, 1999.
50. T. Veijola, "Compact models for squeeze-film dampers with inertial and rarefied gas effects," *J. Micromech. and Microengg.* **14**, pp. 1109–1118, 2004.
51. T. Veijola, H. Kuisma, J. Lahdenpera, and T. Ryhaanen, "Equivalent circuit model of the squeezed gas film in a silicon accelerometer," *Sensors and Actuators A* **48**, pp. 236–248, 1995.
52. I. B. Crandall, "The air damped vibrating system: Theoretical calibration of the condenser transmitter," *Physics Review* **11**, pp. 449–460, 1917.
53. M. Bao, "Energy transfer model for squeeze-film air damping in low vacuum," *J. of Micromech. and Microengg.* **12**, pp. 341–346, 2002.
54. S. S. Mohite, H. Kesari, V. R. Sonti, and R. Pratap, "Analytical solution for the stiffness and damping coefficients of squeeze films in mems devices with perforated back plates," *J. Micromech. and Microengg.* **15**, pp. 2083–2092, 2005.
55. Z. Škvor, "On acoustical resistance due to viscous losses in the air gap of electostatic transducers," *Acustica* **19**, pp. 295–297, 1967–1968.
56. D. Homentcovschi and R. N. Miles, "Modeling of viscous damping of perforated planer microstructures. applications in acoustics," *J. Acoust. Soc. Am.* **116(5)**, pp. 2939–2947, 2004.
57. S. S. Mohite, V. R. Sonti, and R. Pratap, "Analytical model for squeeze-film effects in perforated mems structures including open border effects," in *Proceedings of XX EUROSENSORS 2006*, **II**, pp. 154–155, (Göteborg, Sweden), September 2006.
58. D. Homentcovschi and R. N. Miles, "Viscous damping of perforated planar micromechanicstructures," *Sensors and Actuators A* **119(2)**, pp. 544–552, 2005.
59. M. Bao, H. Yang, Y. Sun, and P. J. French, "Modified reynolds' equation and analytical analysis of squeeze-film air damping of perforated structures," *J. of Micromech and Microengg.* **13**, pp. 795–800, 2003.
60. M. Bao, H. Yang, Y. Sun, and P. J. French, "Squeeze-film air damping of thick hole plate," *Sensors and Actuators A* **108**, pp. 212–217, 2003.
61. T. Veijola and T. Mattila, "Compact squeezed-film damping model for perforated surface," in *Proceedings of Transducers'01*, (München, Germany), June 2001.
62. R. B. Darling, C. Hivick, and J. Xu, "Compact analytical modelling of squeeze film damping with arbitrary venting

conditions using a green's function approach," *Sensors and Actuators A* **70**, pp. 32–41, 1998.
63. P. Y. Kwok, M. S. Weinberg, and K. S. Breuer, "Fluid effects in vibrating micromachined structures," *JMEMS* **14**(4), pp. 770–781, 2005.
64. T. Veijola, "Analytical model for an mem perforation cell," *Microfluidics Nanofluidics* **2**(3), pp. 249–260, 2006.
65. T. Veijola, A. Pursula, and R. back, "Extending the validity of squeeze-film damping models with elongation of surface dimensions," *J. of Micromech and Micrengg.* **15**, pp. 1624–1636, 2004.
66. G. A. Bird, *Molecular Gas Dynamics and the Direct Simulation of Gas Flows*, Oxford University Press, Oxford, 1996.
67. G. E. Karniadakis and A. Beskok, *Micro Flows: Fundamental and Simulation*, Springer-Verlag, New York, 2001.
68. J. B. Starr, "Squeeze-film damping in solid state accelerometers," *Proc. IEEE Solid State Sensors and Actuators Workshop SC USA* , pp. 44–47, 1990.
69. H. Ruth and K. Michael, "Modelling of squeeze-film effects in a mems accelerometer with a levitated proof mass," *J. Micromech. and Microengg.* **15**, pp. 893–902, 2005.
70. H. V. Allen, S. C. Terry, and D. W. De Bruin, "Accelerometer systems with self testable features," *Sensors and Actuators A* **20**, pp. 153–161, 1989.
71. S. S. Mohite, *Study of Squeeze-film Effects in Modelling Dynamic MEMS Devices*. PhD thesis, Department of Mechanical Engineering, Indian Institute of Science, Bangalore, 2006.
72. C. L. Chen and Y. J. Jason, "Damping control of mems devices using structural design approach," *Proc IEEE Solid State Sensors and Actuators Workshop SC USA* , pp. 72–75, 1996.
73. T. Veijola and P. Råback, "A method for solving arbitrary mems problems with rare gas effects," *NSTI-Nanotech* **3**, pp. 561–564, 2005.
74. M. G. Da Silva, "Gas damping and spring effects on mems devices with multiple perforations and multiple gaps," *Proc of Transducers'99* **2**, pp. 1148–1151, 1999.
75. G. Schrag and G. Wachutka, "Physically based modelling of squeeze-film damping by mixed-level system simulation," *Sensors and Actuators A* **97-98**, pp. 193–200, 2002.
76. G. Schrag and G. Wachutka, "Accurate system-level damping model for highly perforated micromechanical devices," *Sensors and Actuators A* **111**, pp. 222–228, 2004.
77. R. Sattler and G. Wachutka, "Analytical compact models for squeezed-film damping," *Proc of DTIP (Montreux)* **111**, pp. 377–382, 2004.
78. P. Råback, A. Persula, V. Junttila, and T. Veijola, "Hierarchical finite element simulation of perforated plates with arbitrary hole geometry," *Proc of the 6th international conference on modelling and simulation of microsystems San Francisco* **1**, pp. 194–197, 2003.
79. R. G. Christian, "Theory of oscillating-vane vaccum gauges," *Vaccum* **16**, pp. 175–178, 1965.
80. J. D. Zook, D. W. Burns, H. Guckel, J. J. Smegowski, and Z. Feng, "Characteristics of polysilicon resonator microbeams," *Sensors and Actuators A* **35**, pp. 51–59, 1992.
81. Z. Kadar, W. Kindt, A. Bossche, and J. Mollinger, "Quality factor of torsional resonators in the low-pressure region," *Sensors and Actuators A* **53**, pp. 299–303, 1996.
82. S. Hutcherson and W. Ye, "On the squeeze-film damping of micro-resonators in the free-molecular regime," *J. of Micromech. and Microengg.* **14**, pp. 1726–33, 2004.
83. A. Minikes, I. Bucher, and G. Avivi, "Damping of a micro-resonator torsion mirror in rarefied gas ambient," *J. of Micromech. and Microengg.* **15**, pp. 1762–69, 2005.
84. E. Kim, Y. Cho, and M. Kim, "Effect of holes and edges on the squeeze film damping of perforated micromechanical structures," in *12th IEEE Intern. Conf. on MEMS (MEMS'99)*, (Orlando, FL), January 1999.
85. A. K. Pandey and R. Pratap, "Studies in non-linear effects of squeeze film damping in mems structures," *International Journal of Computational Engineering Science* **4(3)**, pp. 477–480, 2003.
86. A. K. Pandey and R. Pratap, "Coupled nonlinear effects of surface roughness and rarefaction on squeeze film damping in mems structures," *J. Micromech. and Microengg.* **14**, pp. 1430–1437, 2004.

Prof. Rudra Pratap received his B.Tech. from the Indian Institute of Technology (IIT), Kharagpur in 1985; Masters in mechanics from the University of Arizona, Tucson, in 1987, and Ph.D. in theoretical and applied mechanics from Cornell University in 1993. He taught at Cornell in the Sibley School of Mechanical and Aerospace Engineering during 1993–1996, prior to joining the Indian Institute of Science in 1996. He was also an Adjunct Assistant Professor at Cornell from 1997 to 2000. Presently, he is an Associate Professor in the Department of Mechanical Engineering, Indian Institute of Science, Bangalore, India. His research interests are MEMS design, computational mechanics, nonlinear dynamics, structural vibration and vibroacoustics. Dr. Pratap is a member of IEEE and ISSS and on the Editorial Board of CMC (Journal of Computers, Materials and Continua).

Suhas Mohite received his B.E. from Walchand College of Engineering, Sangli, in 1988; Masters in Machine Tools from the Indian Institute of Technology (IIT), Madras in 1990. After a brief stint in industries and private institutes, he joined as faculty in the Department of Mechanical Engineering, Government College of Engineering, Karad, (M.S.), in 1996. Currently, he is on deputation at the CranesSci MEMS lab. Department of Mechanical Engineering, Indian Institute of Science, Bangalore, where he is working toward the Ph.D. degree. His research interests include design and modelling of acoustical and inertial MEMS.

Ashok Kumar Pandey received his B.E. degree in Mechanical Engineering from Bhilai Institute of Technology, Durg in 2001. He did his Masters in 2003 and presently doing his Ph.D. in MEMS from CranesSci MEMS Lab, Department of Mechanical Engineering, Indian Institute of Science, Bangalore, India. His current research focus is on the investigation of different energy dissipation mechanisms in micro and nano devices.